

VECTOR CIRCUIT THEORY FOR SPATIALLY DISPERSIVE UNIAXIAL MAGNETO-DIELECTRIC SLABS

Pekka Ikonen, Mikhail Lapine, Igor Nefedov, and Sergei Tretyakov

Radio Laboratory/SMARAD, Helsinki University of Technology
P.O. Box 3000, FI-02015 TKK, Finland.

Abstract—We present a general dyadic vector circuit formalism, applicable for uniaxial magneto-dielectric slabs, with strong spatial dispersion explicitly taken into account. This formalism extends the vector circuit theory, previously introduced only for isotropic and chiral slabs. Here we assume that the problem geometry imposes strong spatial dispersion only in the plane, parallel to the slab interfaces. The difference arising from taking into account spatial dispersion along the normal to the interface is briefly discussed. We derive general dyadic impedance and admittance matrices, and calculate corresponding transmission and reflection coefficients for arbitrary plane wave incidence. As a practical example, we consider a metamaterial slab built of conducting wires and split-ring resonators, and show that neglecting spatial dispersion and uniaxial nature in this structure leads to dramatic errors in calculation of transmission characteristics.

- 1 Introduction
- 2 Transmission matrix
- 3 Impedance and admittance matrices
- 4 Reflection and transmission dyadics
- 5 Practically realizable slabs
- 6 Specific examples
- 7 Conclusions

Acknowledgment

References

1. INTRODUCTION

It is well known that many problems dealing with reflections from multilayered media can be solved using the transmission line analogy when the eigen-polarizations are studied separately (see e.g. [1]). In this case, the amplitudes of tangential electric and magnetic fields are treated as equivalent *scalar* voltages and currents in the equivalent transmission line section. In order to account for an arbitrary polarization, Lindell and Alanen introduced a *vector* transmission-line analogy [2], where *vector* tangential electric and magnetic fields serve as equivalent voltage and current quantities. Later on, the vector transmission-line analogy was further extended for isotropic and chiral slabs into a vector circuit formalism, with the slabs represented as two-port circuits with equivalent impedances and admittances [3, 4].

This vector circuit theory has been successfully applied to study plane wave reflection from chiral slabs [5], and extended to uniaxial multilayer structures [6].

Recent emergence of metamaterials and the subsequent growth of research interest to their properties, revitalized the importance of analytical methods for studying artificial media, in particular, for proper calculation of the reflection and transmission properties. The most prominent examples of metamaterials [7] involve split-ring resonators [8] interlayered with a wire structure, being organized in an essentially anisotropic manner (e.g., like shown in Fig. 1a). Effective permittivity (permeability) tensors in such metamaterials correspond to those of uniaxial dielectric (magnetic) crystals, and the principal values of both tensors differ from unity along one direction only. Moreover, the presence of wire medium imposes significant spatial dispersion for all waves with an electric field component along the wires [9].

These peculiarities drive the properties of such metamaterials far apart from what can be described in terms of the isotropic vector circuit theory, and raise a clear demand for an appropriate generalization. The corresponding theory extension is the main objective of this paper.

2. TRANSMISSION MATRIX

Let us consider a spatially dispersive slab having thickness d and characterized by the following material parameter dyadics (Fig. 1b)

$$\bar{\bar{\epsilon}} = \epsilon_t(k_t)\bar{\bar{I}}_t + \epsilon_n\mathbf{nn}, \quad \bar{\bar{\mu}} = \mu_t\bar{\bar{I}}_t + \mu_n\mathbf{nn}, \quad (1)$$

where \mathbf{n} is the unit normal vector for the slab and $\bar{\bar{I}}_t = \bar{\bar{I}} - \mathbf{nn}$ is the transversal unit dyadic. We consider plane wave excitation and move from the physical space to the

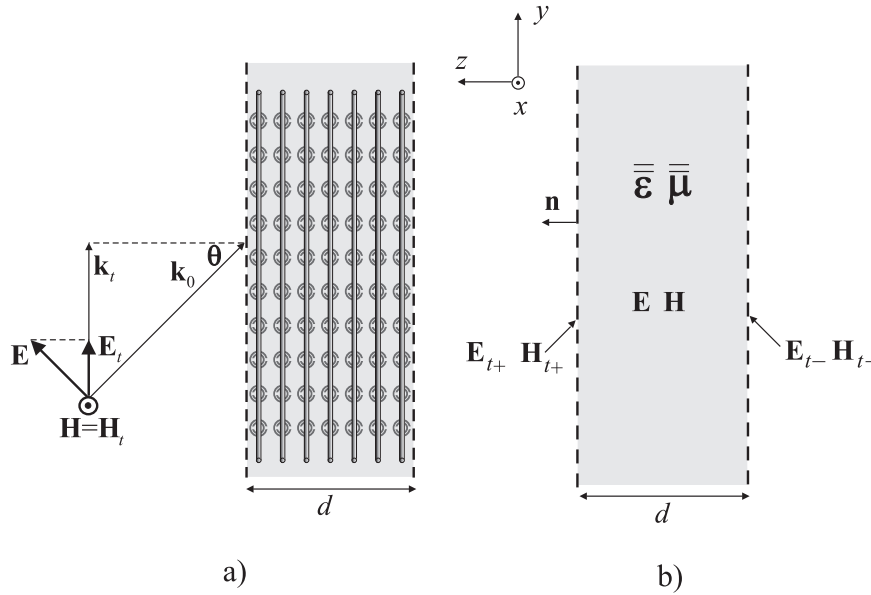


Figure 1. a) A TM-polarized plane wave incident on a slab implemented using an array of wires and split-ring resonators. b) Macroscopic representation of a uniaxial magneto-dielectric slab. Subscripts + and – denote the fields at the left and right sides of the slab, respectively.

Fourier space by a transformation $\nabla_t \rightarrow -j\mathbf{k}_t$. For plane waves, \mathbf{k}_t simply stands for the transversal propagation factor. Physically we could as well assume that the slab is illuminated by a source located electrically far away from the slab. Notation $\epsilon(k_t)$ stresses the spatially dispersive nature of the slab in the tangential plane, and indicates the dependence of the permittivity component from the tangential propagation factor.

Starting from the Maxwell equations the following set of equations can be derived for the tangential field components

$$\frac{\partial}{\partial z} \mathbf{n} \times \mathbf{E}_t = -j\omega\mu_t \mathbf{H}_t + \frac{1}{j\omega\epsilon_n} \mathbf{k}_t \times \mathbf{k}_t \times \mathbf{H}_t, \quad (2)$$

$$\frac{\partial}{\partial z} \mathbf{n} \times \mathbf{H}_t = j\omega\epsilon_t(k_t) \mathbf{E}_t - \frac{1}{j\omega\mu_n} \mathbf{k}_t \times \mathbf{k}_t \times \mathbf{E}_t. \quad (3)$$

Next, we integrate eqs. (2) and (3) over z from 0 to d :

$$\frac{\mathbf{n} \times \mathbf{E}_{t+} - \mathbf{n} \times \mathbf{E}_{t-}}{d} = -j\omega\mu_t \hat{\mathbf{H}}_t + \frac{1}{j\omega\epsilon_n} \mathbf{k}_t \times \mathbf{k}_t \times \hat{\mathbf{H}}_t, \quad (4)$$

$$\frac{\mathbf{n} \times \mathbf{H}_{t+} - \mathbf{n} \times \mathbf{H}_{t-}}{d} = j\omega\epsilon_t(k_t) \hat{\mathbf{E}}_t - \frac{1}{j\omega\mu_n} \mathbf{k}_t \times \mathbf{k}_t \times \hat{\mathbf{E}}_t. \quad (5)$$

Above \mathbf{E}_{t+} , \mathbf{H}_{t+} refer to the fields at the left side of the slab, and \mathbf{E}_{t-} , \mathbf{H}_{t-} refer to the fields at the right side of the slab, Fig. 1a. The averaged fields in eqs. (4) and (5) are defined as

$$\hat{\mathbf{E}}_t = \frac{1}{d} \int_0^d \mathbf{E}_t dz, \quad \hat{\mathbf{H}}_t = \frac{1}{d} \int_0^d \mathbf{H}_t dz. \quad (6)$$

After mathematical manipulation (4) and (5) transform into

$$\mathbf{E}_{t-} - \mathbf{E}_{t+} = -j\omega\mu_t d \bar{\bar{\mathbf{A}}} \cdot \mathbf{n} \times \hat{\mathbf{H}}_t, \quad (7)$$

$$\mathbf{H}_{t-} - \mathbf{H}_{t+} = j\omega\epsilon_t(k_t) d \bar{\bar{\mathbf{B}}} \cdot \mathbf{n} \times \hat{\mathbf{E}}_t. \quad (8)$$

Above dyadics $\bar{\bar{\mathbf{A}}}$ and $\bar{\bar{\mathbf{B}}}$ are defined as

$$\bar{\bar{\mathbf{A}}} = \bar{\bar{\mathbf{I}}}_t - \frac{\mathbf{k}_t \mathbf{k}_t}{\omega^2 \mu_t \epsilon_n} = \frac{\omega^2 \mu_t \epsilon_n - k_t^2}{\omega^2 \mu_t \epsilon_n} \frac{\mathbf{k}_t \mathbf{k}_t}{k_t^2} + \frac{\mathbf{n} \times \mathbf{k}_t \mathbf{n} \times \mathbf{k}_t}{k_t^2}, \quad (9)$$

$$\bar{\bar{\mathbf{B}}} = \bar{\bar{\mathbf{I}}}_t - \frac{\mathbf{k}_t \mathbf{k}_t}{\omega^2 \mu_n \epsilon_t(k_t)} = \frac{\omega^2 \mu_n \epsilon_t(k_t) - k_t^2}{\omega^2 \mu_n \epsilon_t(k_t)} \frac{\mathbf{k}_t \mathbf{k}_t}{k_t^2} + \frac{\mathbf{n} \times \mathbf{k}_t \mathbf{n} \times \mathbf{k}_t}{k_t^2}. \quad (10)$$

The general solution for the transverse electric field inside the slab reads (now the interest lies only on wave propagation in z -direction)

$$\mathbf{E}_t(z) = \mathbf{A} \cdot e^{-j\bar{\beta}z} + \mathbf{B} \cdot e^{j\bar{\beta}z}, \quad (11)$$

where \mathbf{A} and \mathbf{B} are constant vectors and the z -component of propagation factor is different for TM and TE polarizations:

$$\begin{aligned} \bar{\beta} &= \bar{\beta}(k_t) = \beta_{\text{TM}} \frac{\mathbf{k}_t \mathbf{k}_t}{k_t^2} + \beta_{\text{TE}} \frac{\mathbf{n} \times \mathbf{k}_t \mathbf{n} \times \mathbf{k}_t}{k_t^2} \\ &= \sqrt{\frac{\epsilon_t(k_t)}{\epsilon_n} (\omega^2 \mu_t \epsilon_n - k_t^2)} \frac{\mathbf{k}_t \mathbf{k}_t}{k_t^2} + \sqrt{\frac{\mu_t}{\mu_n} (\omega^2 \mu_n \epsilon_t(k_t) - k_t^2)} \frac{\mathbf{n} \times \mathbf{k}_t \mathbf{n} \times \mathbf{k}_t}{k_t^2}. \end{aligned} \quad (12)$$

Constant vectors \mathbf{A} and \mathbf{B} are determined from the boundary conditions

$$\mathbf{E}(0) = \mathbf{E}_{t-}, \quad \mathbf{E}(d) = \mathbf{E}_{t+}, \quad (13)$$

and the following expressions can be derived

$$\mathbf{A} = (e^{-j\bar{\beta}d} - e^{j\bar{\beta}d})^{-1} \cdot (\mathbf{E}_{t+} - \mathbf{E}_{t-} \cdot e^{j\bar{\beta}d}), \quad (14)$$

$$\mathbf{B} = -(e^{-j\bar{\beta}d} - e^{j\bar{\beta}d})^{-1} \cdot (\mathbf{E}_{t+} - \mathbf{E}_{t-} \cdot e^{-j\bar{\beta}d}). \quad (15)$$

After integrating (11) over z from 0 to d we get for the averaged electric field (note that all the dyadics are commutative)

$$\begin{aligned} \hat{\mathbf{E}}_t &= \frac{1}{jd} (\mathbf{E}_{t+} + \mathbf{E}_{t-}) \cdot \bar{\beta}^{-1} \cdot (e^{-j\bar{\beta}d} - e^{j\bar{\beta}d})^{-1} \cdot (2\bar{I}_t - e^{-j\bar{\beta}d} - e^{j\bar{\beta}d}) \\ &= (\mathbf{E}_{t+} + \mathbf{E}_{t-}) \cdot \bar{\beta}^{-1} \cdot \frac{\tan\left(\frac{\bar{\beta}d}{2}\right)}{d}. \end{aligned} \quad (16)$$

Similarly for the magnetic field

$$\hat{\mathbf{H}}_t = (\mathbf{H}_{t+} + \mathbf{H}_{t-}) \cdot \bar{\beta}^{-1} \cdot \frac{\tan\left(\frac{\bar{\beta}d}{2}\right)}{d}. \quad (17)$$

Inserting (16) and (17) into (7) and (8) leads to the following result

$$\mathbf{E}_{t-} - \mathbf{E}_{t+} = -j\omega\mu_t d \bar{\bar{A}} \cdot \mathbf{n} \times (\mathbf{H}_{t+} + \mathbf{H}_{t-}) \cdot \bar{\beta}^{-1} \cdot \bar{f}, \quad (18)$$

$$\mathbf{H}_{t-} - \mathbf{H}_{t+} = j\omega\epsilon_t d \bar{\bar{B}} \cdot \mathbf{n} \times (\mathbf{E}_{t+} + \mathbf{E}_{t-}) \cdot \bar{\beta}^{-1} \cdot \bar{f}. \quad (19)$$

Above we have denoted $\bar{f} = \tan(\bar{\beta}d/2)/d$. Fields at the upper side of the slab can be expressed with the help of the fields at the lower side of the slab and the following result is obtained after mathematical manipulation:

$$\mathbf{E}_{t+} = \cos(\bar{\beta}d) \cdot \mathbf{E}_{t-} + j\omega\mu_t \sin(\bar{\beta}d) \cdot \bar{\beta}^{-1} \cdot \bar{A} \cdot (\mathbf{n} \times \mathbf{H}_{t-}), \quad (20)$$

$$\mathbf{n} \times \mathbf{H}_{t+} = \cos(\bar{\beta}d) \cdot (\mathbf{n} \times \mathbf{H}_{t-}) + j \frac{1}{\omega\mu_t} \sin(\bar{\beta}d) \cdot (\bar{\beta}^{-1} \cdot \bar{A})^{-1} \cdot \mathbf{E}_{t-}. \quad (21)$$

Writing (20) and (21) into a matrix form we identify the dyadic transmission matrix for the slab, Fig. 2a:

$$\begin{pmatrix} \mathbf{E}_{t+} \\ \mathbf{n} \times \mathbf{H}_{t+} \end{pmatrix} = \begin{pmatrix} \bar{\bar{\alpha}}_{11} & \bar{\bar{\alpha}}_{12} \\ \bar{\bar{\alpha}}_{21} & \bar{\bar{\alpha}}_{22} \end{pmatrix} \cdot \begin{pmatrix} \mathbf{E}_{t-} \\ \mathbf{n} \times \mathbf{H}_{t-} \end{pmatrix}, \quad (22)$$

where the transmission components read

$$\bar{\bar{\alpha}}_{11} = \bar{\bar{\alpha}}_{22} = \cos(\beta_{\text{TM}}d) \frac{\mathbf{k}_t \mathbf{k}_t}{k_t^2} + \cos(\beta_{\text{TE}}d) \frac{\mathbf{n} \times \mathbf{k}_t \mathbf{n} \times \mathbf{k}_t}{k_t^2}, \quad (23)$$

$$\bar{\bar{\alpha}}_{21} = j \frac{\omega\epsilon_t(k_t)}{\beta_{\text{TM}}} \sin(\beta_{\text{TM}}d) \frac{\mathbf{k}_t \mathbf{k}_t}{k_t^2} + j \frac{\beta_{\text{TE}}}{\omega\mu_t} \sin(\beta_{\text{TE}}d) \frac{\mathbf{n} \times \mathbf{k}_t \mathbf{n} \times \mathbf{k}_t}{k_t^2}, \quad (24)$$

$$\bar{\bar{\alpha}}_{12} = j \frac{\beta_{\text{TM}}}{\omega\epsilon_t(k_t)} \sin(\beta_{\text{TM}}d) \frac{\mathbf{k}_t \mathbf{k}_t}{k_t^2} + j \frac{\omega\mu_t}{\beta_{\text{TE}}} \sin(\beta_{\text{TE}}d) \frac{\mathbf{n} \times \mathbf{k}_t \mathbf{n} \times \mathbf{k}_t}{k_t^2}. \quad (25)$$

We immediately notice that if the slab is local and isotropic, coefficients (23)–(25) reduce to those obtained earlier for an isotropic slab [3].

The exact boundary condition for a slab on a metal ground plane follows directly from (20) with $\mathbf{E}_{t-} = 0$:

$$\mathbf{E}_{t+} = \bar{\bar{Z}}(k_t) \cdot \mathbf{n} \times \mathbf{H}_{t+}, \quad (26)$$

where the impedance operator reads

$$\bar{\bar{Z}}(k_t) = j \frac{\beta_{\text{TM}}}{\omega \epsilon_t(k_t)} \tan(\beta_{\text{TM}} d) \frac{\mathbf{k}_t \mathbf{k}_t}{k_t^2} + j \frac{\omega \mu_t}{\beta_{\text{TE}}} \tan(\beta_{\text{TE}} d) \frac{\mathbf{n} \times \mathbf{k}_t \mathbf{n} \times \mathbf{k}_t}{k_t^2}. \quad (27)$$

3. IMPEDANCE AND ADMITTANCE MATRICES

From (22) it is straightforward to derive the impedance and admittance matrices for the slab

$$\begin{pmatrix} \mathbf{E}_{t+} \\ \mathbf{E}_{t-} \end{pmatrix} = \begin{pmatrix} \bar{\bar{Z}}_{11} & \bar{\bar{Z}}_{12} \\ \bar{\bar{Z}}_{21} & \bar{\bar{Z}}_{22} \end{pmatrix} \cdot \begin{pmatrix} \mathbf{n} \times \mathbf{H}_{t+} \\ \mathbf{n} \times \mathbf{H}_{t-} \end{pmatrix}, \quad (28)$$

$$\begin{pmatrix} \mathbf{n} \times \mathbf{H}_{t+} \\ \mathbf{n} \times \mathbf{H}_{t-} \end{pmatrix} = \begin{pmatrix} \bar{\bar{Y}}_{11} & \bar{\bar{Y}}_{12} \\ \bar{\bar{Y}}_{21} & \bar{\bar{Y}}_{22} \end{pmatrix} \cdot \begin{pmatrix} \mathbf{E}_{t+} \\ \mathbf{E}_{t-} \end{pmatrix}, \quad (29)$$

where the dyadic impedances and admittances depend on the transmission components in the following way

$$\bar{\bar{Z}}_{11} = \bar{\bar{\alpha}}_{11} \cdot \bar{\bar{\alpha}}_{21}^{-1}, \quad \bar{\bar{Z}}_{12} = -\bar{\bar{\alpha}}_{11} \cdot \bar{\bar{\alpha}}_{21}^{-1} \cdot \bar{\bar{\alpha}}_{22} + \bar{\bar{\alpha}}_{12}, \quad (30)$$

$$\bar{\bar{Z}}_{21} = \bar{\bar{\alpha}}_{21}^{-1}, \quad \bar{\bar{Z}}_{22} = -\bar{\bar{\alpha}}_{21}^{-1} \cdot \bar{\bar{\alpha}}_{22}, \quad (31)$$

$$\bar{\bar{Y}}_{11} = \bar{\bar{\alpha}}_{22} \cdot \bar{\bar{\alpha}}_{12}^{-1}, \quad \bar{\bar{Y}}_{12} = \bar{\bar{\alpha}}_{21} - \bar{\bar{\alpha}}_{22} \cdot \bar{\bar{\alpha}}_{12}^{-1} \cdot \bar{\bar{\alpha}}_{11}, \quad (32)$$

$$\bar{\bar{Y}}_{21} = \bar{\bar{\alpha}}_{12}^{-1}, \quad \bar{\bar{Y}}_{22} = -\bar{\bar{\alpha}}_{12}^{-1} \cdot \bar{\bar{\alpha}}_{11}. \quad (33)$$

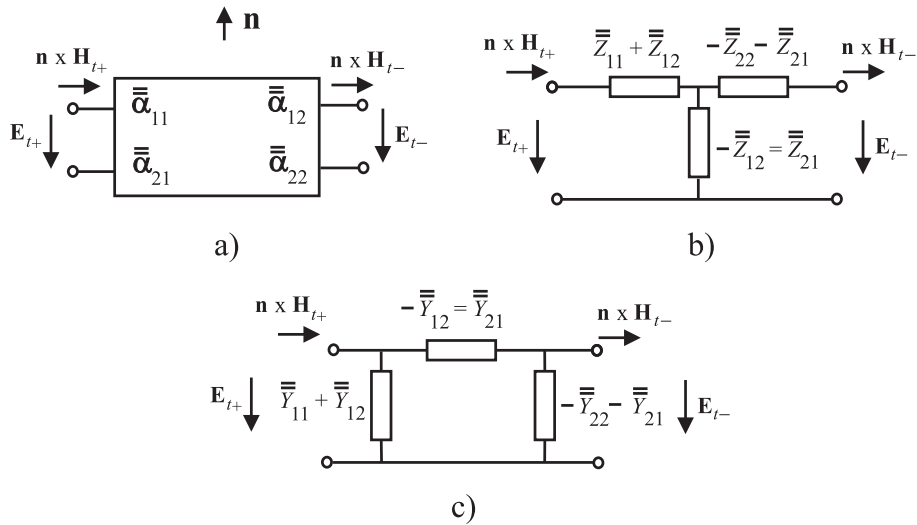


Figure 2. Different representations for the slab: a) A two-port transmission line section. b) Vector T-circuit. c) Vector Π -circuit. The orientation of the unit vector \mathbf{n} is in all the cases the same as depicted in a).

The corresponding T and $\mathsf{\Pi}$ -circuit representations are presented in Fig. 2b and Fig. 2c, respectively.

4. REFLECTION AND TRANSMISSION DYADICS

Introducing dyadic reflection and transmission coefficients $\overline{\overline{R}}$ and $\overline{\overline{T}}$, eq. (22) can be written as two equations in the following form:

$$(\overline{\overline{I}}_t + \overline{\overline{R}}) \cdot \mathbf{E}_t^{\text{inc}} = \overline{\overline{\alpha}}_{11} \cdot \overline{\overline{T}} \cdot \mathbf{E}_t^{\text{inc}} + \overline{\overline{\alpha}}_{12} \cdot \overline{\overline{Z}}_0^{-1} \cdot \overline{\overline{T}} \cdot \mathbf{E}_t^{\text{inc}}, \quad (34)$$

$$\overline{\overline{Z}}_0^{-1} \cdot (\overline{\overline{I}}_t - \overline{\overline{R}}) \cdot \mathbf{E}_t^{\text{inc}} = \overline{\overline{\alpha}}_{21} \cdot \overline{\overline{T}} \cdot \mathbf{E}_t^{\text{inc}} + \overline{\overline{\alpha}}_{22} \cdot \overline{\overline{Z}}_0^{-1} \cdot \overline{\overline{T}} \cdot \mathbf{E}_t^{\text{inc}}, \quad (35)$$

where $\mathbf{E}_t^{\text{inc}}$ denotes the incoming electric field and $\overline{\overline{Z}}_0$ is the free space impedance dyadic (seen by the tangential fields)

$$\overline{\overline{Z}}_0 = \eta_0 \cos \theta \frac{\mathbf{k}_t \mathbf{k}_t}{k_t^2} + \frac{\eta_0}{\cos \theta} \frac{\mathbf{n} \times \mathbf{k}_t \mathbf{n} \times \mathbf{k}_t}{k_t^2}. \quad (36)$$

From eqs. (34) and (35) we can readily solve the transmission and reflection dyadics:

$$\overline{\overline{T}} = 2(\overline{\overline{\alpha}}_{11} + \overline{\overline{\alpha}}_{22} + \overline{\overline{\alpha}}_{12} \cdot \overline{\overline{Z}}_0^{-1} + \overline{\overline{Z}}_0 \cdot \overline{\overline{\alpha}}_{21})^{-1} \cdot \overline{\overline{I}}_t, \quad (37)$$

$$\overline{\overline{R}} = (\overline{\overline{\alpha}}_{11} + \overline{\overline{\alpha}}_{12} \cdot \overline{\overline{Z}}_0^{-1}) \cdot \overline{\overline{T}} - \overline{\overline{I}}_t. \quad (38)$$

5. PRACTICALLY REALIZABLE SLABS

A typical example which fits into the general model presented above, is a slab of metamaterial, implemented as an array of conducting wires and split rings resonators (WM-SRR structure), Fig 1a. The wires are assumed to be infinitely long in the y -direction. Moreover, the number of wires in the x -direction, and the number of split-ring resonators both in the x - and y -directions is assumed to be infinite.

For the case shown in Fig. 1a the non-local permittivity dyadic reads [9]

$$\overline{\overline{\epsilon}} = \epsilon_x \mathbf{u}_x \mathbf{u}_x + \epsilon_y \mathbf{u}_y \mathbf{u}_y + \epsilon_z \mathbf{u}_z \mathbf{u}_z, \quad (39)$$

$$\epsilon_x = \epsilon_z = \epsilon_h, \quad \epsilon_y = \epsilon_h \left(1 - \frac{k_p^2}{k^2 - k_y^2} \right), \quad (40)$$

where ϵ_h is the permittivity of the host matrix, k_p is the plasma wave number, k is the wave number of the host medium, and k_y is the y -component of the wave vector inside the lattice. Generalization of the dyadic for a case when the wires are periodically arranged along two directions (double-wire medium with non-connected wires [10]) is straightforward.

A commonly accepted permeability model as an effective medium description of dense (in terms of the wavelength) arrays of split-ring resonators (SRRs) and other similar structures reads (see e.g. [11, 12, 13])

$$\overline{\overline{\mu}} = \mu_x \mathbf{u}_x \mathbf{u}_x + \mu_y \mathbf{u}_y \mathbf{u}_y + \mu_z \mathbf{u}_z \mathbf{u}_z, \quad (41)$$

$$\mu_x = \mu_h \left(1 + \frac{\Lambda \omega^2}{\omega_0^2 - \omega^2 + j\omega\Gamma} \right), \quad \mu_y = \mu_z = \mu_h, \quad (42)$$

where μ_h is the permeability of the host medium, Λ is the amplitude factor ($0 < \Lambda < 1$), ω_0 is the undamped angular frequency of the zeroth pole pair (the resonant frequency of the array), and Γ is the loss factor. These parameters can be theoretically estimated for any particular case [12]. When the SRRs are positioned to the locations where the quasi-static magnetic field produced by the wires is zero (to the symmetry planes), there is no near field coupling between the two fractions [14] and the whole metamaterial can be characterized by the permittivity and permeability in the form above.

The derivation presented above holds for the WM-SRR structure only when the wires are parallel to the slab interfaces and the tangential propagation factor is restricted to the interval $0 \leq k_t < k$. In this case a plane wave incident on the slab excites only TM and TE wave. If the slab is excited by a source, located close to the surface, or the source is inside the slab, an additional TEM wave will be excited by the source, [9]. The same happens for an incident plane wave, if $k_t = k$. Note that, when the wires are perpendicular to the interface different approach is needed. Recently, authors of [15] considered a slab with wires perpendicular to the interfaces and presented another method to calculate the transmission coefficient for such a slab.

6. SPECIFIC EXAMPLES

Here we present some calculated results for plane wave transmission through the WM-SRR slab in Fig. 1b. We compare the transmission coefficient calculated when the slab is assumed to be uniaxial and non-local with the transmission coefficient obtained when: (i) the slab is assumed to be uniaxial but local, or (ii) the slab is assumed to be isotropic and local. Local model for the permittivity means that $k_y = 0$ in (40). Next, we study the angular dependence of the transmission coefficient at certain frequencies when the effective refractive index of the slab is close to zero. For simplicity, only an example of TM polarization is considered.

For this analysis we assume the following parameters: slab thickness $d = 150$ mm, $\epsilon_h = \epsilon_0$, and $k_p = 104.7 \text{ m}^{-1}$ (the corresponding plasma frequency is $f_p = 5$ GHz); $\mu_h = \mu_0$, $\Lambda = 0.4$, $\omega_0 = 2\pi \cdot 2.5$ GHz, $\Gamma = \omega_0/50$. The permittivity and permeability dyadics are calculated in accordance with equations (39)–(40) and (41)–(42), respectively.

Fig. 3 compares the exact transmission coefficient to the transmission coefficient calculated when the slab is assumed to be local [case (i)]. Only for the normal incidence (not plotted) the results are the same. At small incidence angles (e.g. $\theta = \pi/6$) there is a transmission maximum around 3 GHz. This maximum corresponds to the frequency range where both $\text{Re}\{\epsilon\}$ and $\text{Re}\{\mu\}$ are negative and relatively close to unity in magnitude. In this situation a planar slab can bring a point source to a focus without spherical aberration [16]. In a certain frequency above 3 GHz $\text{Re}\{\mu\}$ becomes positive while $\text{Re}\{\epsilon\}$ remains negative, leading to a stop-band. At frequency $f = f_p$ permittivity becomes positive and waves can propagate through the slab. Note that when the permittivity is assumed to be non-local the position of the pass-band edge is predicted at remarkably higher frequencies compared to the local model.

For larger incidence angles (e.g. $\theta = \pi/3$) the maxima around 3 GHz disappear and the transmission coefficient obeys an increasing behavior starting at f_0 (the resonant frequency for μ_t). Indeed, eq. (12) for β_{TM} shows that the term $\text{Re}\{k_0^2(\mu_t - \sin^2\theta)\}$ is negative at frequencies $f > f_0$. Thus, a pass-band will appear in the frequency interval $f_0 < f < f_p$ because in this interval also $\text{Re}\{\epsilon\}$ is negative.

Fig. 4 compares the exact transmission coefficient to the transmission coefficient calculated when the slab is assumed to be local and isotropic [case (ii)]. Clearly the

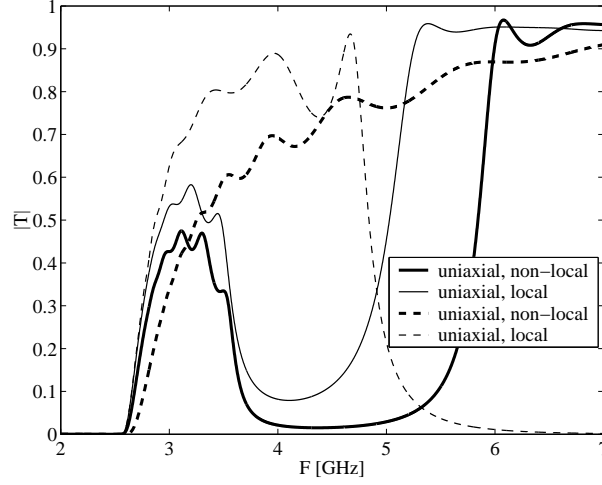


Figure 3. Transmission coefficient (absolute value) as a function of frequency at different incidence angles. Exact transmission coefficient (thick lines) is compared to the transmission coefficient calculated using local permittivity model (thin lines). Solid lines: $\theta = \pi/6$, dashed lines: $\theta = \pi/3$.

assumption that the slab is isotropic and local leads to severe errors except for the normal incidence.

For an additional illustration we study the angular dependence of the transmission coefficient at certain frequencies when the effective refractive index n of the slab is close to zero while $\text{Re}\{\mu_t\} > 0 \wedge \text{Re}\{\mu_t\} \neq \mu_0$, and $\text{Re}\{\epsilon_t\} > 0 \wedge \text{Re}\{\epsilon_t\} \neq \epsilon_0$. Comparison is made between the results given by the non-local and local models (in both models the slab is assumed to be uniaxial). An interest to this problem arises from recent suggestions for microwave applications benefiting from slabs having low value for both $\text{Re}\{\mu\}$ and $\text{Re}\{\epsilon\}$ [17].

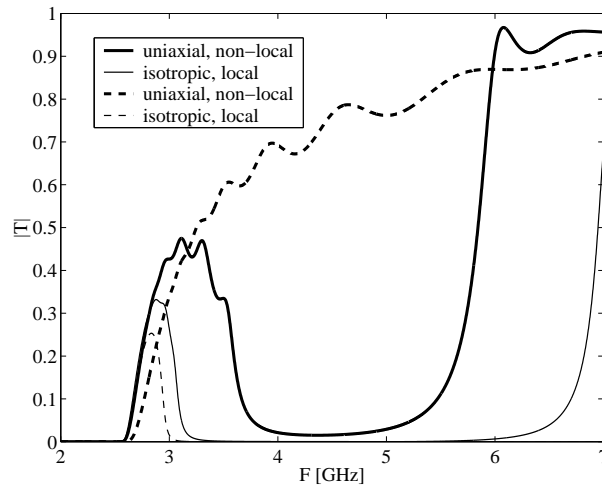


Figure 4. Transmission coefficient (absolute value) as a function of frequency at different incidence angles. Exact transmission coefficient (thick lines) is compared to the transmission coefficient calculated using local and isotropic permittivity model (thin lines). Solid lines: $\theta = \pi/6$, dashed lines: $\theta = \pi/3$.

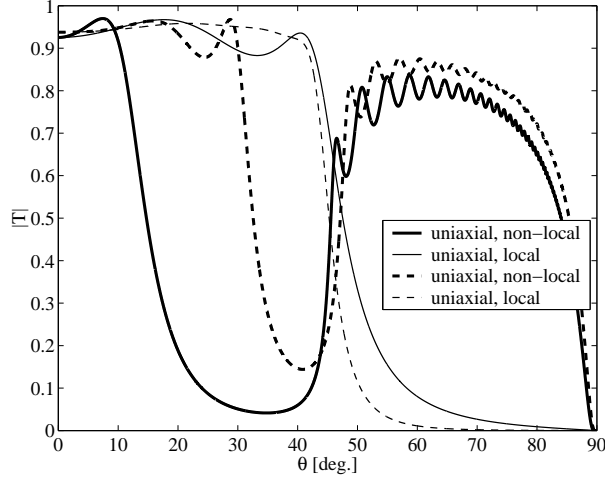


Figure 5. Transmission coefficient (absolute value) as a function of the incidence angle at certain frequencies. Exact transmission coefficient (thick lines) is compared to the transmission coefficient calculated using local permittivity model (thin lines). Solid lines: $f = 1.05 \times f_p$, dashed lines $f = 1.20 \times f_p$.

In practise the condition $n \approx 0$, $\text{Re}\{\mu_t\} > 0 \wedge \text{Re}\{\epsilon_t\} > 0$ occurs at frequencies slightly above f_p . We have to bear in mind, however, the physical limitation of the permeability model (42): the model is valid at low frequencies and at frequencies relatively close to the magnetic resonance. Here we assume that in the vicinity of f_p the permeability model is still valid. The transmission coefficients are depicted in Fig. 6. It shows that transmission maxima, covering a wide range of angles from 50 to 80 degrees appear when the non-local model is used. These maxima are not predicted when the local permittivity model is used. This behavior can be explained by considering the z -component of the propagation factor, which in this case can be written in the following form:

$$\frac{\beta_{\text{TM}}^2}{k_0^2} = \left(1 - \frac{k_p^2}{k_0^2 \cos^2 \theta} \right) (\mu_t - \sin^2 \theta). \quad (43)$$

In order for a wave to propagate through the slab, both terms inside the parentheses [the right side of eq. (43)] must be simultaneously positive or negative. For small incidence angles both are positive and for large angles both are negative. In a certain range of angles, however, these terms are of opposite sign, leading to a stop-band.

Effectively condition $n \approx 0$ can also be achieved in photonic crystals in the vicinity of the stop-band edge, e.g. [18, 19, 20]. This feature is reported to be important for practical applications (e.g. [21]). Accordingly, we can apply the developed method to study the transmission characteristics of the slab only in the presence of wires. Fig. 5 shows the calculated results (note the range of incidence angles). The transmission maxima seen at certain angles correspond to thickness resonances of the slab. The results indicate that the slab can be utilized as an effective angular filter at microwave frequencies. Note that when the permittivity is assumed to be local, some maxima are also seen in the transmission coefficient, however, the location of these maxima is incorrectly predicted.

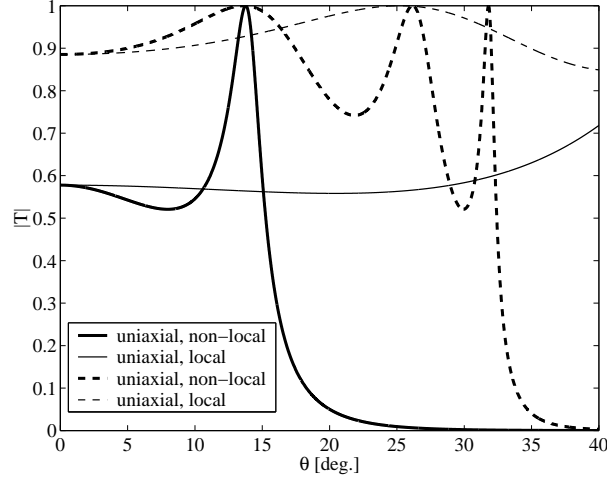


Figure 6. Transmission coefficient (absolute value) as a function of the incidence angle at certain frequencies when the slab is assumed to consist only of wires. Exact transmission coefficient (thick lines) is compared to the transmission coefficient calculated using local permittivity model (thin lines). Solid lines: $f = 1.05 \times f_p$, dashed lines $f = 1.20 \times f_p$.

7. CONCLUSIONS

In this paper we have formulated a vector circuit representation for spatially dispersive uniaxial magneto-dielectric slabs. A dyadic transmission matrix and the corresponding impedance and admittance matrices have been derived. The results take into account spatial dispersion along the planes parallel to the slab interfaces.

The presented results allow the exact calculation of the transmission and reflection coefficient for a plane wave with arbitrary incidence angles. This model is applicable, for example, to a typical metamaterial implemented as a lattice of conducting wires and split-ring resonators. It has been shown that for accurate transmission analysis the uniaxial nature of such a slab, and the spatial dispersion in the wire media must be taken into account. The calculated results also indicate the feasibility of the slab to operate as an effective angular filter at microwave frequencies.

ACKNOWLEDGMENT

This work has been done within the frame of the European Network of Excellence *Metamorphose*. The authors wish to thank Professor Constantin Simovski and Dr. Ari Viitanen for stimulating discussions.

REFERENCES

1. L. B. Felsen and N. Marcuvitz, *Radiation and scattering of waves*, Piscataway, NJ: IEEE Press, 1991.
2. I. V. Lindell and E. Alanen, "Exact image theory for the Sommerfeld half-space problem, part III: General formulation," *IEEE Trans. Antennas Propagat.*, Vol. AP-32, 1027–1032, Oct. 1984.

3. M. I. Oksanen, S. A. Tretyakov, I. V. Lindell, "Vector circuit theory for isotropic and chiral slabs," *J. Electromagnetic Waves Appl.*, Vol. 4, 613–643, 1990.
4. S. Tretyakov, *Analytical modeling in applied electromagnetics*, Norwood, MA: Artech House, 2003.
5. A. J. Viitanen and P. P. Puska, "Reflection of obliquely incident plane wave from chiral slab backed by soft and hard surface," *IEE Proc. Microwaves, Antennas and Propagat.*, Vol. 146, 271–276, Aug. 1999.
6. A. Serdyukov, I. Semchenko, S. Tretyakov, A. Sihvola, *Electromagnetics of bi-anisotropic materials; Theory and applications*, Gordon and Breach Science Publishers, 2001.
7. D. R. Smith, W. J. Padilla, D. C. Vier, S. C. Nemat-Nasser, and S. Schultz, "Composite medium with simultaneously negative permeability and permittivity," *Phys. Rev. Lett.*, Vol. 84, 4184–4187, May 2000.
8. J. B. Pendry, A. J. Holden, D. J. Robbins, and W. J. Stewart, "Magnetism from conductors and enhanced nonlinear phenomena," *IEEE Trans. Microwave Theory Tech.*, Vol. 47, 2075–2084, Nov. 1999.
9. P. A. Belov, R. Marqués, S. I. Maslovski, I. S. Nefedov, M. Silveirinha, C. R. Simovski, S. A. Tretyakov, "Strong spatial dispersion in wire media in the very large wavelength limit," *Phys. Rev. B*, Vol. 67, 113103, March 2003.
10. I. S. Nefedov, A. J. Viitanen, S. A. Tretyakov, "Electromagnetic wave refraction at an interface of a double wire medium," *Phys. Rev. B*, Vol. 72, 245113, 2005.
11. M. V. Kostin and V. V. Shevchenko, "Artificial magnetism based on double circular elements," *Proc. Bianisotropics'94*, 49–56, Périgueux, France, May 18–20, 1994.
12. M. Gorkunov, M. Lapine, E. Shamonina, and K. H. Ringhofer, "Effective magnetic properties of a composite material with circular conductive elements," *Eur. Phys. J. B*, Vol. 28, 263–269, July 2002.
13. S. I. Maslovski, P. Ikonen, I. A. Kolmakov, S. A. Tretyakov, M. Kaunisto, "Artificial magnetic materials based on the new magnetic particle: Metasolenoid," *Progress in Electromagnetics Research*, Vol. 54, 61–81, 2005.
14. S. I. Maslovski, "On the possibility of creating artificial media simultaneously possessing negative permittivity and permeability," *Techn. Phys. Lett.*, Vol. 29, 32–34, Jan. 2003.
15. P. A. Belov and M. G. Silveirinha, "Resolution of sub-wavelength lenses formed by the wire medium," arXiv:physics/0511139, Feb. 2006.
16. J. B. Pendry, "Negative refraction makes a perfect lens," *Phys. Rev. Lett.*, Vol. 85, 3966–3969, Oct. 2000.
17. N. Engheta, M. Silveirinha, A. Alu, A. Salandrino, "Scattering and reflection properties of low-epsilon metamaterials shells and bends", *Proc. of joint ICEAA'05 and EESC'05 Conf.*, 101–104, Torino, Italy, Sept. 12–16, 2005.
18. B. Gralak, S. Enoch, G. Tayeb, "Anomalous refractive properties of photonic crystals," *J. Opt. Soc. Am. B*, Vol. 17, 1012–1020, June 2000.
19. N. Garcia, E. V. Ponizovskaya, J. Q. Xiao, "Zero permittivity materials: Band gaps at the visible," *Appl. Phys. Lett.*, Vol. 80, 1120–1122, Feb. 2002.
20. B. T. Schwartz and R. Piestun, "Total external reflection from metamaterials with ultralow refractive index," *J. Opt. Soc. Am. B*, Vol. 20, 2448–2453, Dec. 2003.
21. S. Enoch, G. Tayeb, P. Sabouroux, N. Guérin, P. Vincent, "A metamaterial for directive emission," *Phys. Rev. Lett.*, Vol. 89, 213902(-1-4), Nov. 2002.